Evaluating the Structural Response of Ceramic-Metal Laminate under Ballistic Impact

Mohd Suhairil Meon[*]*, Muhammad Qmie Delfrin, Juri Saedon*
School of Mechanical Engineering, College of Engineering,
Universiti Teknologi MARA, 40450 Shah Alam, Selangor, MALAYSIA
[*]*msuhairil@uitm.edu.my*

ABSTRACT

Ceramics are widely employed in armor because of their toughness, but their susceptibility to fractures under high-speed impact poses a challenge. To address this gap, a comprehensive investigation using finite element analysis is undertaken. This study aims to understand the combined behaviour of ceramics and backing plates during ballistic impact. Using ABAQUS software, a range of simulations are conducted involving circular ceramics paired with different types of backing plate, considering varying impact energies. The results revealed that the integrity of the ceramic-metal laminate structure is highly dependent on the laminate configurations. From four combinations of hybrid laminates, the combination of boron carbide with Armox 500T as the backing plate produced an outstanding result based on the structural response analysed in this work. The key results obtained provide valuable insights into the response of ceramic-armored configurations, filling a critical knowledge gap.

Keywords: *Ballistic Impact; Finite Element Analysis; Ceramic; Backing Plate; Impact Energy*

Introduction

Ceramic materials have received significant attention in the armour area due to their exceptional combination of durability and hardness, which allows them to withstand and disperse the initial movement energy from ballistic impacts. However, despite these advantages, ceramics are known to exhibit inherent brittleness, making them susceptible to fragmentation and failure when exposed to high-speed projectiles. This vulnerability underscores the need to

ISSN 1823-5514, eISSN 2550-164X
Received for review: 2023-09-06
Accepted for publication: 2024-01-26
Published: 2024-04-15

https://doi.org/10.24191/jmeche.v21i2.26257

understand the complex interactions between ceramics and other materials in protective systems. In response, research efforts have turned to finite element analysis, a powerful computational tool that provides insight into the dynamic behaviour of materials exposed to impact forces. By simulating ballistic scenarios, researchers can precisely study the mechanical reactions of ceramics and their interactions with supporting materials, highlighting factors that contribute to their performance and potential failure modes. This research line has great promise in advancing the development of effective armament solutions to protect personnel and property in environments characterised by ballistic threats, from military combat to civilian security applications.

In many previous studies, researchers have extensively investigated ceramics to understand how they responded to ballistic impacts when used in armour systems [1]. To address the challenges posed by the low fracture toughness and limited tensile strength of ceramics, a solution emerged: the integration of ductile backing plates to enhance the mechanical properties of ceramics [2]. Important attributes of the ceramic material such as hardness, flexural strength, fracture toughness, and Young's modulus were considered [3]. In terms of the ballistic performance of the armor structure, multiple factors were found to influence it, as highlighted by the research by Guo, Alam, and Peel [4], including material characteristics, specimen dimensions, bonding layer characteristics, projectile shape, impact velocities, and boundary conditions.

Bresciani et al. [5] explored the mechanical attributes of alumina ceramic and tungsten alloy in projectiles. Their work uncovered that surface waves transformed into tensile waves, causing radial fractures upon impact. In parallel investigations, Armox 500T steel as backing and alumina ceramic Al_2O_3 as front plate were studied by Zochowski et al. [6] and Gositanon et al. [7] to analyse the focus of kinetic energy during ballistic impact. Furthermore, interactions between ceramics and hardened steel 4340 projectiles were examined by some researchers [2], [8]-[9]. Goda and Giradot [10] assessed the effects of ballistic impact on alumina and WFRP materials at various velocities. Grujicic et al. [11] explored the role of polyurea as an adhesive layer between alumina and a polymer back plate, observing reduced stress in the adhesive and ceramic sections of the hybrid armor. Dresch et al. [1] evaluated ceramics mechanical characteristics and their influence on dynamic ballistic performance, noting the role of the elastic modulus in improving energy absorption. Other researchers studied ceramic Al_2O_3 as the front layer and different aluminium properties as the back plate [12]-[15]. Guo et al. [4] evaluated a model with a ceramic-filled honeycomb and Kevlar-29 backing, while Mahfuz et al. [16] investigated the response of an armor system to ballistic impact and found that the initial compression stress changed to tensile stress, illuminating material behavior during ballistic events.

Building on previous investigations, ceramic analysis often relies on the Johnson-Holmquist damage model, recognised for its applicability to capture

the mechanical response of materials with high compressive strength and low tensile strength and the inherent characteristics of ceramics [2], [4], [6], [9], [12]. This model finds widespread use in achieving precise numerical simulations of armor penetration arising from ballistic impacts [7], [11], [13]-[14]. In addition, the Johnson-Holmquist 2 model (JH-2) emerges as a valuable tool to depict the behaviour of ceramics under conditions of high strain rates, shear strain, and pressure induced by ballistic impacts [10], [15]. Comprising three essential components, the JH-2 model encompasses a pressure-dependent yield surface, accounting for intact and fractured strength, a damage model simulating the transition from an intact to a fractured state for ceramic materials, and an equation of state (EOS) that defines the pressure-volume relationship.

However, the interaction between ballistic speed and hybrid laminate configuration remains a subject of research interest as a result of the complex interaction between them and the damage morphology, and this interaction is still poorly understood. This work examines the impact of a hybrid laminate combination between metal and ceramics at different impact velocities on the responses to structural integrity. In this paper, a robust three-dimensional (3D) model is developed using ABAQUS software, where the main case study is obtained from several prominent journals. The investigation involves a comprehensive range of tests that cover four distinct impact energy levels, involving various ceramics and backing plate setups. To predict ceramic failure, the study employs the Johnson-Holmquist 2 (JH-2) formulation, while the behaviour of the backing plate is modelled using the Johnson-Cook (JC) approach. The primary metrics of the study include depth of penetration (DOP), residual velocity, and energy absorption, providing a comprehensive evaluation of ballistic performance. Additionally, the analysis explores the consequential impact of erosion on material integrity, adding depth to understanding ballistic interactions. These findings not only contribute to optimising armour design, but also have implications for enhancing protective systems in scenarios involving ballistic threats.

Methodology

In this section, details of the finite element models for the three different components utilised are introduced. This included the projectile, the ceramic plate, and the FRP composite laminate. These components were established and merged within ABAQUS/CAE, and the ABAQUS/Explicit solver was used to process the entire simulation. Additionally, a quarter model was created to enhance computational efficiency and conserve computational resources due to the model's symmetry about both the X-axis and the Y-axis.

Finite element model

The entire analysis in this research was carried out using a 3D numerical simulation model implemented in Abaqus/Explicit environment. Both the projectile and the plate were represented by quarter-models and each model was simulated as a deformable material. The adoption of quarter models allowed for a reduction in overall analysis time [17]. The backing and ceramic plate were meshed with a three-dimensional 8-noded linear brick (C3D8R), using reduced integration and hourglass control elements, with a finer mesh size of 1mm x 1mm x 0.8mm at the centre. This mesh size was chosen after performing several tests and referring to the available literature [17] to prevent distorted elements resulting from ballistic impact. The remaining area was meshed with a three-dimensional 8-noded linear brick (C3D8R), with a mesh size of 1 x 1 x 1 mm. For the tungsten projectile, a three-dimensional 8-noded linear brick mesh (C3D8R) was employed, integrating reduced integration, hourglass control, and a global mesh size of 1.2 mm using solid elements. The complete finite element models for both the plate and the impactor are shown in Figure 1.

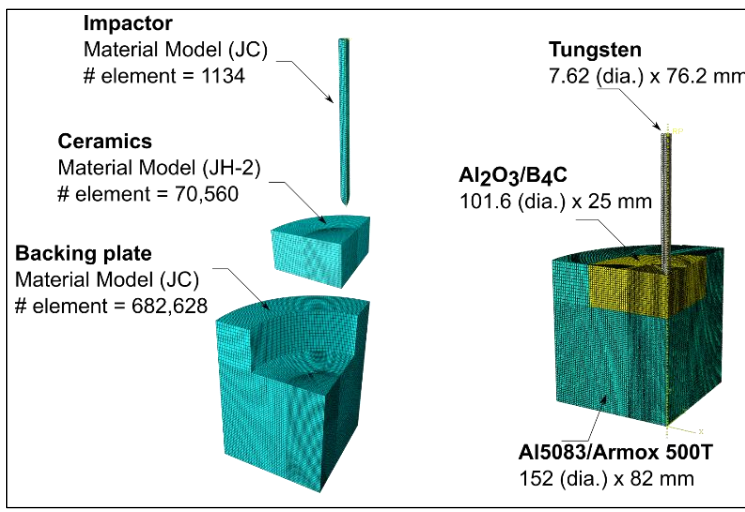

Figure 1: Test specimen including material model and number of elements used in this project

The interaction employed between the backing plate and the ceramic plate consisted of automatic surface-to-surface interaction and a tie constraint. This interaction was applied to ensure an even load distribution across the contact area of the backing plate and the ceramic plate. Regarding the projectile and target, eroding surface-to-surface contact was used, designating

the target elements as masters and the projectile as slaves. The set of surfaces used for the target and the projectile in this interaction was defined through geometry and selected from all entities to facilitate the erosion process. To allow the projectile to move along with velocity, an equation-type constraint was used between the projectile and a reference point, considering that the load is applied at this reference point. Since the quarter model was used in this project, the boundary condition of symmetry in the x and y axes as depicted in Figure 2 was applied to enhance the computational time.

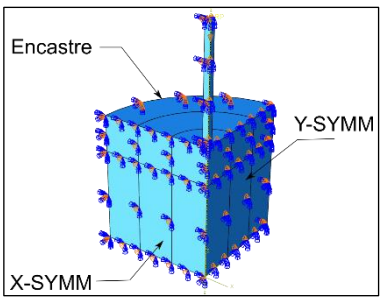

Figure 2: The boundary conditions of the quarter model

Mathematical model

In this simulation, two mathematical/constitutive models, namely Johnson-Holmquist 2 (JH-2) and Johnson-Cook (JC), were utilized. The selection of these damage models was driven by their alignment with the ceramics and metals used in the simulation, ensuring the accuracy of the results.

Johnson-Holmquist 2

To characterise the ceramic materials, namely alumina (Al_2O_3) and boron carbide (B_4C), a constitutive model was used, specifically the Johnson-Holmquist (JH-2) model [17], to study ballistic impact. The JH-2 model comprises three primary components: a pressure-dependent yield surface depicting the strength of both intact and fractured material, a damage model facilitating the progressive transformation from an intact to a fractured state, and an equation of state that delineates the pressure-density relationship. The strength of the material equivalent to stress can be expressed as:

$$\sigma^* = \sigma_i^* - D\left(\sigma_i^* - \sigma_f^*\right) \tag{1}$$

where σ^* is normalized strength equivalent stress, σ_i^* and σ_f^* are the normalized intact equivalent stress and the normalized fracture equivalent stress, respectively while D is the damage parameter. The normalized intact and for the fracture strength is given by:

$$\sigma_i^* = A(P^* + T^*)^N(1 + C\ ln\ \dot{\varepsilon}^*) \quad (2)$$

$$\sigma_f^* = B(P^*)^M(1 + C\ ln\ \dot{\varepsilon}^*) \quad (3)$$

where *A, B, C, N, M* are the material parameters and $\dot{\varepsilon}^*$ is the actual strain rate. As for P^* and T^* are the material specific constant and normalized by equivalent pressure at Hugoniot elastic limit, P_{HEL} as written below.

$$P^* = \frac{P}{P_{HEL}} \quad (4)$$

$$T^* = \frac{T}{P_{HEL}} \quad (5)$$

$$\dot{\varepsilon} = \frac{\varepsilon}{\varepsilon_0} \quad (6)$$

where P is the actual pressure and T is the maximum hydrostatic tensile pressure that the material can sustain. ε_0 is the reference strain rate, usually it set to $1.0\ s^{-1}$ [11].

The damage parameter of the JH-2 model quantifies the extent of material degradation or damage. Typically measured within a range of 0 to 1, where 0 signifies an intact material and 1 indicates complete failure or fragmentation. Alterations in the damage parameter occur as the material undergoes plastic deformation, taking into account factors such as strain, strain rate, and fracture characteristics of the material. This can be elaborated as follows:

$$D = \sum \frac{\Delta\varepsilon_p}{\varepsilon_p^f} \quad (7)$$

where $\Delta\varepsilon_p$ is the increment n equivalent plastic strain and the equivalent fracture strain at failure strain ε_p^f can be determine by:

$$\varepsilon_p^f = D_1(P^* + T^*)^{D_2} \quad (8)$$

where D_1 and D_2 are the material constant. The material properties used in this article are shown in Table 1.

Table 1: JH-2 properties [17]

Parameters	Symbol (unit)	Al_2O_3	B_4C
Density	ρ *(kg/mm³)*	*3.9e-6*	*2.5e-6*
Shear modulus	*G (GPa)*	*135*	*197*
Intact strength constant	*A* (GPa)	0.987	0.927
Fracture Strength Constant	*B* (GPa)	0.77	0.7
Strain rate constant	*C*	0	0.005
Fracture strength exponent	*M*	1	0.85
Intact strength exponent	*N*	0.376	0.67
Max. fracture strength ratio	Sf_{max}	0.5	0.2
Hugoniot elastic limit	*HEL*	5.9	19
Pressure at HEL	P_{HEL} (GPa)	2.2	8.71
Melting temperature	T_m (GPa)	0.15	0.26
Ref. strain rate	ε	1	1
Damage parameter	D_1	0.01	0.001
	D_2	1	0.5
Max. effective strain at failure	EFF_EPS	2	2.1
Bulking constant	BETA	1	1
Failure strain	FS	1.5	1.5
Bulk modulus	K_1 (GPa)	200	233

Johnson-Cook

For characterizing the materials employed in the backing plate and projectile, including Aluminium 5083 (Al5083), Armox 500T steel, and Tungsten, the constitutive model selected was Johnson-Cook (JC). The rationale behind opting for the JC model is based on its ability to describe material behaviour under high strain rates during ballistic impact analysis. Moreover, this model incorporates considerations of yielding, hardening, plastic flow, and strain rate hardening and softening. The von-Mises flow stress for metal:

$$\sigma = [A + B(\bar{\varepsilon}^{pl})^N][1 + C\left(\frac{\dot{\bar{\varepsilon}}^{pl}}{\dot{\varepsilon_0}}\right)][1 - \hat{T}^M] \tag{9}$$

$$\hat{T} = \frac{T - T_{room}}{T_{melt} - T_{room}} \tag{10}$$

where *A* is the yield strength, *B* is the strengthening constant, *C* is the strain rate constant, *N* is the strengthening exponent, *M* is the thermal softening factor, $\bar{\varepsilon}^{pl}$ is the effective plastic strain, $\dot{\bar{\varepsilon}}^{pl}$ is the strain rate, $\dot{\varepsilon_0}$ is the reference value for the strain rate, $\hat{T}$ is the dimensionless temperature, T_{room} is the room temperature, T_{melt} is the melting temperature and *T* is the current temperature.

The accumulation of damage is realised using an equation similar to JH-2 as in Equation (7). The plastic strain to failure for metals has been related to various parameters as follows:

$$\bar{\varepsilon}_f^{pl} = \left[D_1 + D_2 \exp\left(D_3 \frac{\sigma_m}{\bar{\sigma}}\right)\right]\left[1 + D_4 \ln\left(\frac{\dot{\bar{\varepsilon}}^{pl}}{\dot{\varepsilon}_0}\right)\right]\left[1 + D_5 \hat{T}\right] \qquad (11)$$

where σ_m is the mean stress and $\bar{\sigma}$ is the von-misses stress. All the JC parameters for Al 5083 and tungsten are derived from [17] while for the ARMOX 500T steel is obtained from [6]. Table 2 presents a tabulated compilation of parameter values and term definitions related to Equation (11).

Table 2: JC properties [6], [17]

Parameters	Symbol (unit)	Al 5083	Tungsten	ARMOX 500T
Density	ρ (kg/mm^3)	2.7e-6	17.6e-6	7.85e-6
Elastic modulus	E (GPa)	70	314	210
Shear modulus	G (GPa)	26.9	160	-
Poisson's ratio	μ	0.3	0.29	0.33
Yield stress	A (GPa)	0.167	1.506	1.580
Strengthening constant	B (GPa)	0.596	0.177	0.756
Strain rate constant	C	0.001	0.0016	0.005
Thermal softening constant	M	0.859	1	0.81
Strengthening exponent	N	0.551	0.12	0.199
Melting temperature	T_m (K)	893	1723	1800
Room temperature	T_r (K)	300	300	-
Specific heat	C_p (J/Kg.K)	910	134	4770
Damage parameter	D_1	0.0261	0.5	0.068
	D_2	0.263	0.5	5.32
	D_3	-0.349	-1.5	-2.55
	D_4	0.247	0	0.016
	D_5	16.79	0	1.10
Max. effective strain at failure	EFFEPS	2	1.5	1
Bulk modulus	K_1 (GPa)	58.3	-	-

Numerical modelling strategy

The simulations were carried out using four different impact energy that was applied on each of four different models. This makes it possible to determine with accuracy how each model performs under different impact energies and to examine how the projectile reacts at different material of the model. Table 3 shows the test matrix for the whole simulation. Since the primary focus of this study was to assess the performance of the ceramics and the backing plate, the projectile material remained constant throughout the simulation.

Table 3: Detail planning for the simulation

Sequence	Initial velocity (m/s)	Impactor	Ceramics	Backing plate
1	1000	Tungsten	Al_2O_3	Al 5083
2	1250			
3	1800			
4	2000			
5	1000	Tungsten	B_4C	Al 5083
6	1250			
7	1800			
8	2000			
9	1000	Tungsten	Al_2O_3	Armox T500
10	1250			
11	1800			
12	2000			
13	1000	Tungsten	B_4C	Armox T500
14	1250			
15	1800			
16	2000			

Results and Discussion

Numerical simulations are conducted to thoroughly examine the damage behaviours of the ceramic and backing plate responses resulting from ballistic impacts. These impacts encompass various impact energies, converted into initial velocities, and their responses are assessed through examination of the depth of penetration, energy dissipation history curves, and acquired damage data. In addition, a comprehensive investigation on the influence of ceramics and backing plate materials on the residual velocity of the projectile is carried out.

Mesh sensitivity analysis

The accuracy of the simulation results depended greatly on the shape and size of the mesh. Figure 3 shows the impact of a tungsten projectile travelling at 1800 m/s on an Al_2O_3/Al5083 model using three different mesh sizes. It was observed that utilising a finer mesh led to increased penetration depth, which, in turn, enhanced the force and energy transfer upon impact. However, although finer meshes provide more precise results, they also increase the total number of elements in the model, resulting in longer simulation times and an increase in CPU usage. Therefore, a compromise needs to be considered, which balances the need for greater accuracy with the efficient use of computational resources.

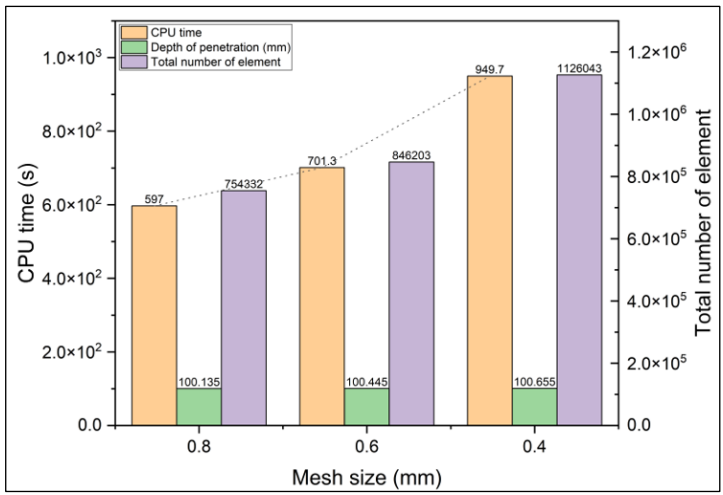

Figure 3: Results for mesh convergence analysis

As a result, 0.8 mm mesh sizes were chosen for all models, taking into account a 0.3% difference in penetration depth. Since the study was limited to a total of 16 tests, it was necessary to assign priority to quickly complete simulations, although smaller mesh sizes would provide greater accuracy. Furthermore, the use of a finer mesh had no effect on the other outcomes except to modify the depth of penetration and prolong the overall duration of the simulation.

Numerical validation

The models were validated with verified numerical or experimental results from respected publications to ensure the feasibility of the current models. Both Al_2O_3/Al5083 and B_4C/Al5083 models simulated with impact energies of 878 m/s and 1550 m/s, respectively, as shown in Table 4. Analysis showed that B_4C/Al5083 models are deeper penetration at the initial speed of 878 m/s, and with a difference of 15% relative to experimental data, and a difference of about 9% relative to Rathod's results [13]. On the contrary, Al_2O_3/Al5083 simulation results support the idea of a slight deeper penetration, with a difference of less than 2% compared to experimental and verified simulation results. The variation in the simulation result can be attributed to the lack of reference paper-specific fracture energy properties and the use of more precise meshes by the authors, which resulted in a larger number of elements. Overall, however, the results indicated acceptable differences, confirming the success of the simulation.

Table 4: Validation of experimental results with numerical results

Initial velocity (m/s)	Hybrid laminate							
	Al_2O_3/Al5083				B_4C/Al5083			
	Exp. (mm)	Num. (mm) [13]	Current (mm)	Error* (%)	Exp. (mm)	Num. (mm) [13]	Current (mm)	Error* (%)
878	-	-			39	41	45	15.4
1550	87.8	90	89	1.37	-	-		

*Comparison between the current model and the experimental data.

Residual velocity

Residual velocity played a crucial role in ballistics tests, serving as a vital parameter for evaluating the effectiveness of model material, optimising the design, and obtaining data for the development of protective measures. The results presented in Table 5 indicate an average reduction in reduction in velocity of 28.5% to reach the residual velocity. It is widely observed in ballistic research that materials with higher hardness and strength tend to exhibit lower residual velocities.

Table 5: Comparison of the residual velocity under different sets of armor specimens and initial velocities

Initial velocity (m/s)	Residual velocity (m/s)			
	Al_2O_3/ Al5083	Al_2O_3/ Armox 500T	B_4C/ Al5083	B_4C/ Armox 500T
1000	769.41	657.71	765.84	654.05
1250	1016.72	809.27	1009.30	809.67
1800	1492.92	1032.51	1508.15	1060.15
2000	1689.83	1138.20	1686.38	1088.70

Regarding the models that employ alumina and boron carbide with an aluminium backing plate, the mean percentage velocity was 19% higher than the residual velocity. However, a comparison between these models revealed that B_4C/Al5083 exhibited a lower residual velocity than Al_2O_3/Al5083. This discrepancy can be attributed to the superior material properties of boron carbide, including its higher hardness and strength relative to those of alumina. These attributes enable boron carbide to absorb kinetic energy more effectively, resulting in a lower residual velocity.

On the contrary, when Armox 500T was used as a backing plate, the results of Table 5 demonstrate that the alumina model exhibited a smaller residual velocity compared to the boron carbide model. This disparity can be linked to the behaviour of the Al_2O_3/Armox 500T model upon projectile impact. Alumina, which is more susceptible to deformation and fracture,

experienced a greater dissipation of kinetic energy during the penetration process. Consequently, the model absorbed a significant portion of the projectile's energy, resulting in a diminished residual velocity. On the other hand, the B_4C/Armox 500T model, characterized by its higher hardness and strength, exhibited greater resistance to deformation and fracture upon impact. As a result, it absorbed less kinetic energy from the projectile, leading to a higher residual velocity compared to the Al_2O_3/Armox 500T model.

Depth of penetration

The depth of penetration among the four models displayed significant variations in the simulation, as illustrated in Figure 4. To evaluate penetration depth, impact energies of 1000 m/s, 1250 m/s, 1800 m/s and 2000 m/s were utilised. In terms of the selected impact energy, both Al_2O_3/Al5083 and B_4C/Al5083 exhibited significant variations in the depth of penetration. However, the difference between the two materials was relatively small, ranging from 0.1 mm to 2 mm, making it difficult to identify a clear distinction based only on the simulation results. However, the properties of hardness and strength play a crucial role in explaining this disparity. Alumina, with a Mohs hardness of 9, and boron carbide, closer to 9.5, indicate that boron carbide possesses a higher resistance to deformation and greater energy absorption capabilities compared to alumina. Despite the fact that alumina has a higher density than boron carbide, its exceptional hardness and structural durability compensate for the density differential. Furthermore, the lower density of the boron carbide contributes to its lightweight nature, which is advantageous for applications requiring a reduction of weight.

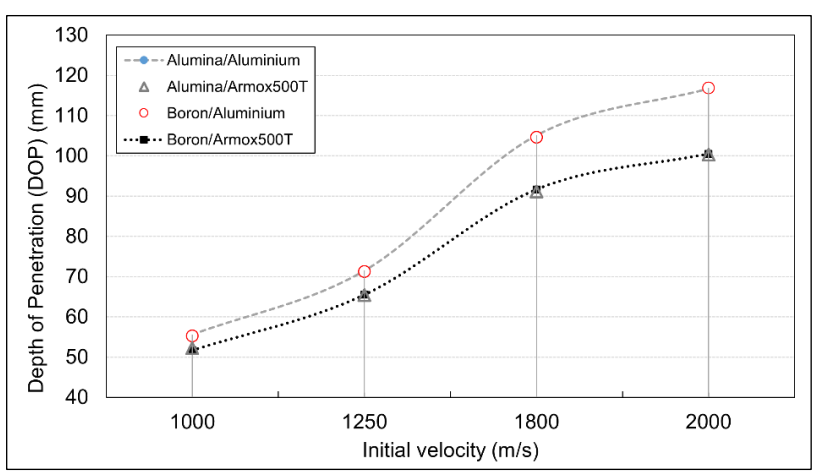

Figure 4: Comparison of depth of penetration (DOP) on different types of combination and reference

However, the result was significantly influenced by the substitution of the Al5083 backing plate from Al5083 to Armox 500T. When steel was utilized as the backing plate in the model, there was a notable 15% reduction in the depth of penetration in the highest velocity due to the change in backing plate material. The significant difference in penetration can be seen in Figure 5. This decrease can be attributed to the exceptional strength, toughness, and hardness of Armox 500T, enabling it to withstand substantial impact energy. In comparison, aluminium 5083 has a lower hardness and density than Armox 500T. The superior properties of Armox 500T allow it to resist deformation and absorb significant energy, thereby preventing the projectile from fully penetrating. Although the characteristics of aluminium are advantageous in specific applications where energy absorption through plastic deformation is desired, they can result in deeper penetration compared to Armox 500T.

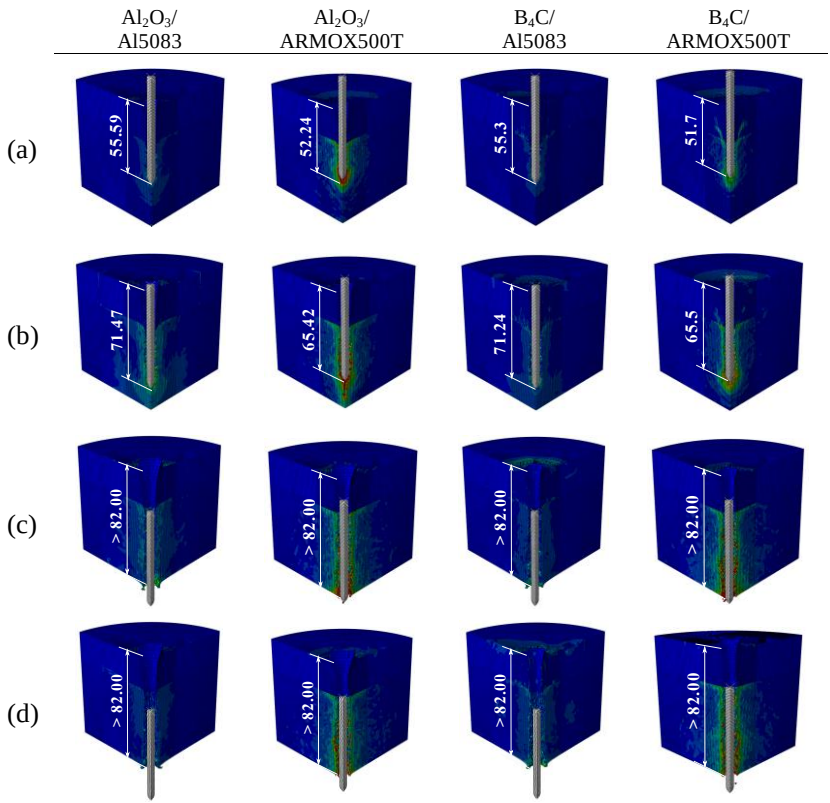

Figure 5: Visualisation of depth of penetration (DOP) for different ceramic/metal combination at the end of calculation time for (a) 1000 m/s, (b) 1250 m/s, (c) 1800 m/s, and (d) 2000 m/s (measurement in mm)

Kinetic energy and energy absorption

Figure 6 displays the kinetic energy (KE) of four distinct models for each initial velocity. It clearly demonstrates an evident trend where the kinetic energy decreases with the extension of time. This behaviour can be attributed to the transmission of kinetic energy from the projectile to the target model during the penetration process as can be seen in several publications [13], [18]-[19]. As the projectile continues to penetrate, its kinetic energy gradually decreases until its velocity reaches zero, indicating the complete transfer of the kinetic energy to the model. Thus, the model experiences an increase in internal energy, while its kinetic energy declines. The penetration modes of two kinds of targets are elaborated in detail in the work of Tan et al. [20], and correlates well with the evidence provided in this paper.

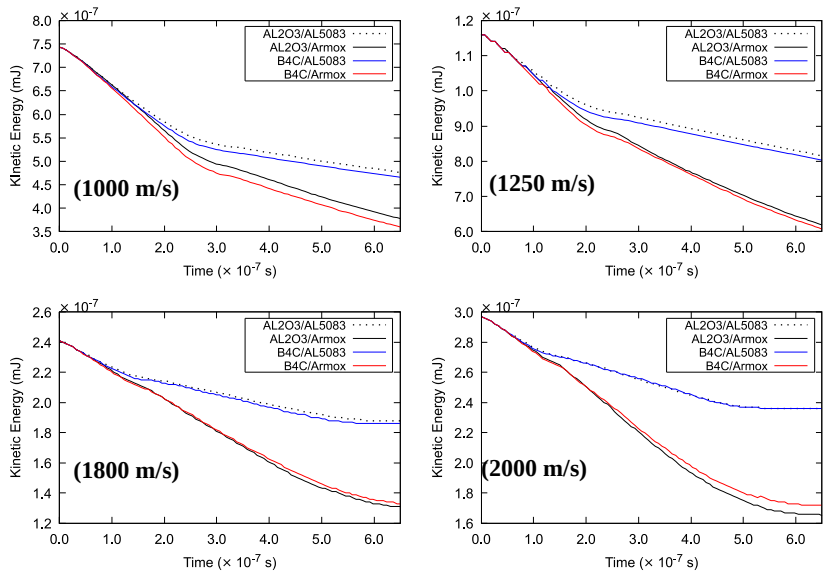

Figure 6: Kinetic energy responses with time for different types of combination and initial velocities

The difference in kinetic energy between the Armox 500T and aluminium 5083 backing plates is striking, as depicted in Figure 4. The models using these materials showed a substantial difference of 33% in kinetic energy. This discrepancy arises from the superior strength and hardness of Armox 500T, which allows it to withstand deformation and fracture caused by impact. Consequently, Armox 500T achieves penetration completion earlier than aluminium 5083, enabling it to absorb a greater amount of kinetic energy from the projectile, and consequently increasing the internal energy. On the other

hand, aluminium 5083, while still capable of energy absorption, is more prone to deformation and flow under impact. This leads to a higher conversion of kinetic energy to internal energy. In contrast, Armox 500T exhibits less deformation and higher absorption of kinetic energy, resulting in a lesser conversion of kinetic energy to internal energy.

Kinetic energy responses have been transformed into energy absorption rates. A higher energy absorption rate in the composite structure indicates better ballistic performance. Therefore, based on the calculated kinetic energy, we have acquired the energy absorption rates (EA) for four different types of ceramic/metal structure under various initial impact velocities (1000 m/s, 1250 m/s, 1800 m/s and 2000 m/s), and the comparison results are presented in Table 6. The results indicate that when combined with Al_2O_3 or B_4C, the Armox 500T backing plate produces the highest energy absorption rate. However, when coupled with an Al5083 plate, the EA rate decreases by nearly half for higher impact energies (1800 m/s and 2000 m/s). Once again, it is worth noting that the steel plate outperforms the aluminium plate in terms of absorption rate and density. Overall, it is evident that the EA rate increases with increasing initial velocity magnitude, irrespective of the ceramic-metal combination plates.

Table 6: Energy absorption calculated from kinetic energy

Initial velocity (m/s)	Energy absorption (J)			
	Al_2O_3/ Al5083	Al_2O_3/ Armox 500T	B_4C/ Al5083	B_4C/ Armox500T
1000	2665.19	3645.9	2766.88	3827.12
1250	3447.08	5415064	3571.87	5531.16
1800	5277.6	10998.8	5499.3	10734.3
2000	6138.5	13168.1	6150.5	12615.9

Damage mechanisms of ceramic/metal

During the ballistic impact simulation, the projectile strikes the ceramic plate and subsequently penetrates the backing plate. Initially, the ceramic front plate offers resistance to the projectile, leading to a reduction in its penetration depth and kinetic energy. The damage observed on the ceramic front surface is a result of the pressure generated during impact between the projectile and the target, as documented in reference [7]. Consequently, the ceramics experience failure, which permits the projectile to penetrate deeper. Following the ceramics' failure, the projectile maintains a consistent velocity until it reaches the backing plate.

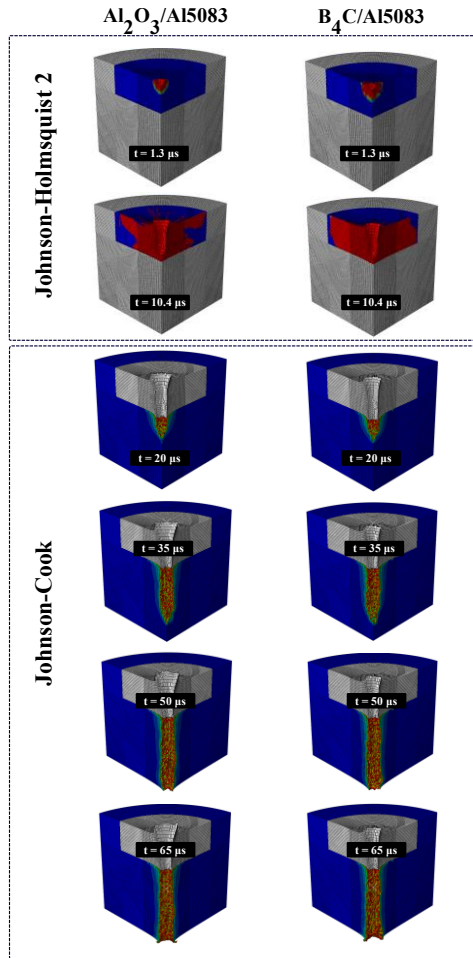

Figure 7: Damage morphology between ceramics materials Al_2O_3 and B_4C coupled with Al5083 backing plate for an initial velocity of 2000 m/s

Figure 7 shows the progression of the damage while increasing the impacted time at an initial speed of 2000 m/s. For this case, a comparison was made between Al_2O_3/Al5083 and B_4C/Al5083 to assess the occurrence of damage using a similar backing plate (Aluminium). In the figure, the fully damaged elements are highlighted in red, whereas the undamaged elements are shown in blue. Additionally, areas shaded grey are not related to the dedicated damage model. When the projectile hits the target, boron ceramics exhibit earlier penetration compared to alumina ceramics. The activation of the JH-2 criteria is used to predict the failure of the element according to its theoretical

framework. In particular, boron ceramics produce a damaged area larger than that of alumina ceramics. A larger von Mises stress area in the model signifies its ability to absorb a higher kinetic energy, indicating that Al_2O_3 has a lower ability to absorb kinetic energy despite its lower density compared to boron carbide. The superior hardness of boron carbide contributes to its enhanced kinetic energy absorption. Interestingly, although boron carbide has a smaller density than alumina, it demonstrates superior kinetic energy absorption capabilities. Similar damage patterns observed upon entering the backing plate zone suggest that the primary function of the plate is to absorb high energy and decelerate the projectile.

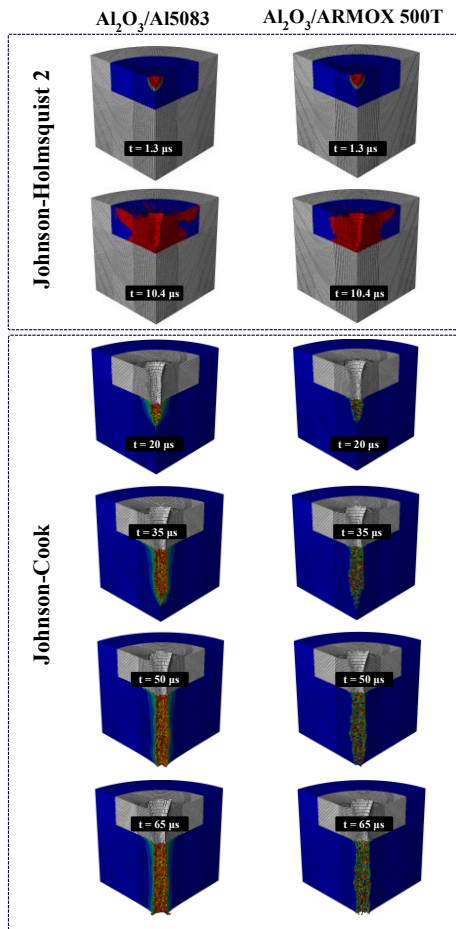

Figure 8: Damage morphology between ceramic material Al_2O_3 coupled with Al5083/Armox 500T backing plate for an initial velocity of 2000 m/s

Figure 8 presents the impact of the backing plate on the damage morphology of the ceramic-metal hybrid plate. It is noteworthy that when the projectile penetrates the metal plate, both materials attempt to resist the striker's motion. The projectile undergoes significant deformation primarily due to the model's hardness. This deformation becomes more pronounced during high-impact energy events and deeper penetrations, as the target absorbs energy from the projectile. At the 20 μs mark, the damaged areas in aluminium are wider than those in Armox steel. This trend persists in other timestamps, clearly demonstrating that steel outperforms aluminium as an energy absorption material. Furthermore, the higher density of Armox 500T compared to aluminium 5083 leads to less deformation and higher stress.

Conclusions

This work establishes finite element analysis of different to evaluate their ballistic performances when impacted by various velocities. The performance of alumina and boron carbide models against tungsten projectiles at different velocities exhibited remarkable similarity. However, despite both ceramics using the same backing plate and other constant conditions, boron carbide showed slightly superior performance, with a 0.3% advantage over alumina. The relationship between hardness, strength, and the depth of penetration was observed, highlighting the need to consider multiple properties when assessing the ballistic performance of ceramics and backing plates. It became evident that no single property alone can accurately determine the effectiveness of a ceramic and backing plate set-up in ballistic impact scenarios. These findings underscore the importance of considering various factors in ballistic impact analysis.

After evaluating the overall results, the Armox 500T (steel) backing plate exhibited the best performance compared to other combination of models. This superior performance can be attributed to the exceptional hardness and strength properties of the boron carbide model, which minimized deformation and allowed for greater absorption of kinetic energy from the projectile. This study highlights the need to compare different materials. Therefore, it is suggested to use boron carbide and Armox 500T for armour applications.

In conclusion, the integrity of the ceramic-metal laminate structure is based on the laminate configurations. A key determinant is the hardness of the selected materials, with a higher hardness enhancing the structure's ability to absorb energy, thereby gradually reducing projectile penetration depth and significantly improving the ballistic performance of the hybrid laminate in various scenarios.

Contributions of Authors

The authors confirm the equal contribution in each part of this work. All authors reviewed and approved the final version of this work.

Funding

This work was supported by Geran Penyelidikan Khas (GPK) from Universiti Teknologi MARA (UiTM) [600-RMC/GPK 5/3 (151/020)].

Conflict of Interests

All authors declare that they have no conflicts of interest.

Acknowledgment

The authors express their gratitude to the staff of the School of Mechanical Engineering, College of Engineering, UiTM for technical support and Research Management Institute UiTM for financial assistance.

References

[1] A. B. Dresch, J. Venturini, S. Arcaro, O. R. K. Montedo, and C. P. Bergmann, "Ballistic ceramics and analysis of their mechanical properties for armour applications: A review", *Ceramics International*, vol. 47, no. 7, pp. 8743-8761, 2021.

[2] M. K. Khan, M. A. Iqbal, V. Bratov, N. F. Morozov, and N. K. Gupta, "An investigation of the ballistic performance of independent ceramic target", *Thin-Walled Structures*, vol. 154, pp. 1-15, 2020.

[3] I. A. Shah, R. Khan, S. S. Rahimian Koloor, M. Petrů, S. Badshah, S. Ahmad, and M. Amjad, "Finite element analysis of the ballistic impact on auxetic sandwich composite human body armor", *Materials*, vol. 15, no. 6, pp. 1-16, 2022.

[4] G. Guo, S. Alam, and L. D. Peel, "Numerical analysis of ballistic impact performance of two ceramic-based armor structures", *Composites Part C: Open Access*, vol. 3, pp. 1-10, 2020.

[5] L. M. Bresciani, A. Manes, and M. Giglio, "An analytical model for ballistic impacts against ceramic tiles", *Ceramics International*, vol. 44, no. 17, pp. 21249–21261, 2018.

[6] P. Zochowski, M. Bajkowski, R. Grygoruk, M. Magier, W. Burian, D. Pyka, M. Bocian, and K. Jamroziak, "Comparison of numerical simulation techniques of ballistic ceramics under projectile impact conditions", *Materials*, vol. 15, no. 1, pp. 1-22, 2021.

[7] A. Gositanon, M. Chaiyarit and S. Phabjanda, "Ballistic Simulation and Verification of Ceramic/rubber Composite Armour," *6th International Conference on Mechanical, Automotive and Materials Engineering (CMAME)*, Hong Kong, China, pp. 18-22, 2018.

[8] D. P. Gonçalves, F. C. L. De Melo, A. N. Klein, and H. A. Al-Qureshi, "Analysis and investigation of ballistic impact on ceramic/metal composite armour," *International Journal of Machine Tools and Manufacture*, vol. 44, no. 2–3, pp. 307–316, 2004.

[9] M. K. Khan and M. A. Iqbal, "Failure and fragmentation of ceramic target with varying geometric configuration under ballistic impact*," Ceramics International*, vol. 48, no. 18, pp. 26147–26167, 2022.

[10] I. Goda and J. Girardot, "Numerical modeling and analysis of the ballistic impact response of ceramic/composite targets and the influence of cohesive material parameters," *International Journal of Damage Mechanics*, vol. 30, no. 7, pp. 1079-1122, 2021.

[11] M. Grujicic, B. Pandurangan, and B. d'Entremont, "The role of adhesive in the ballistic/structural performance of ceramic/polymer-matrix composite hybrid armor", *Materials & Design*, vol. 41, pp. 380–393, 2012.

[12] S. Stanisławek, A. Morka, and T. Niezgoda, "Numerical analysis of an influence of ceramic plate surrounding by metal components in a ballistic panel," *Journal of KONES*, vol. 18, no. 4, pp. 471-474, 2011.

[13] M. Garcia-Avila, M. Portanova, and A. Rabiei, "Ballistic performance of composite metal foams", *Composite Structures*, vol. 125, pp. 202–211, 2015.

[14] A. Prakash, J. Rajasankar, N. R. Iyer, N. Anandavalli, S. K. Biswas, and A. K. Mukhopadhyay, "Prediction of behavior of ceramic/metal composite panels under two consecutive ballistic impacts," *International Journal for Computational Methods in Engineering Science and Mechanics*, vol. 15, no. 3, pp. 192-202, 2014.

[15] V. S. Gálvez and L. S. Paradela, "Analysis of failure of add-on armour for vehicle protection against ballistic impact", *Engineering Failure Analysis*, vol. 16, no. 6, pp. 1837-1845, 2009.

[16] H. Mahfuz, Y. Zhu, A. Haque, A. Abutalib, U. Vaidya, S. Jeelani, B. Gama, J. Gillespie, and B. Fink, "Investigation of high-velocity impact on integral armor using finite element method," *International Journal of Impact Engineering*, vol. 24, no. 2, pp. 203-217, 2000.

[17] S. Rathod, G. Tiwari, and D. Chougale, "Ballistic performance of ceramic–metal composite structures," *Materials Today: Proceedings*, vol. 41, pp. 1125-1129, 2021.

[18] T. Akbari, A. Ansari, and M. Rahimi Pishbijari, "Influence of aluminum alloys on protection performance of metal matrix composite armor reinforced with ceramic particles under ballistic impact", *Ceramics International*, vol. 49, no. 19, pp. 30937-30950, 2023.

[19] J. Xu, L. Tang, Y. Liu, L. Zhou, J. Chen, Z. Jiang, Z. Liu, and B. Yang, "Hybridization effects on ballistic impact behavior of carbon/aramid fiber reinforced hybrid composite," *International Journal of Impact Engineering*, vol 181, pp. 2023, 104750.

[20] M. Tan, X. Zhang, W. Xiong, C. Liu, G. Han, and Y. Li, "Influence of layered back plate on the ballistic performance of ceramic armor", *Composite Structures*, vol. 308, p. 116688, 2023.